https://doi.org/10.1016/j.apacoust.2017.07.018

Optimization of geometrical parameters for periodical structures applied to floating raft systems by genetic algorithms

Zhen Wang, Cheuk Ming Mak *

Department of Building Services Engineering, The Hong Kong Polytechnic University, Hung Hom, Kowloon, Hong Kong

*Corresponding Author: Tel.: +852 2766 5856; Fax: +852 2765 7198

E-mail address: cheuk-ming.mak@polyu.edu.hk (C.M. Mak).

ABSTRACT: This paper presented a theoretical study of the vibration control of a floating raft system using periodic structures. The band gap properties of the periodic structures, the power flow and the power transmissibility of the floating raft system were investigated by using the transfer matrix method. To minimize the power flow through periodic structures in a floating raft system, the geometrical parameters of the periodic structures were optimized by using a genetic algorithm. The numerical results demonstrated that the optimum periodic structure can provide broader stop band regions. The stop band regions of the optimum periodic structure contained all the harmonic frequencies of the force excitation in the floating raft system. The numerical results validated that the proposed optimization approach is sufficiently capable for the design of periodic structures. The proposed optimization approach has potential use for the development of vibration and shock isolation systems such as floating raft systems.

Keywords: Vibration isolation; Periodic structure; Geometric optimization; Genetic algorithms; Floating raft;

1. Introduction

The floating raft systems, a kind of two-stage vibration isolation system, have been widely applied to ships and submarines to improve acoustic stealth performances [1, 2]. Rotatory machines such as: diesel engines, pumps, and electric generators were installed on floating raft systems. Noise and vibration of rotatory machines were generally dominated by peaks at the rotational frequency, blade pass frequency, and their various harmonics in the frequency spectra. Therefore, in the design of noise and vibration systems, more concerns were focused on these frequencies.

Comprehensive efforts have been made in the investigation of the propagation of waves in periodic structures that consisted of several identical structural components [3-5]. Waves transmitted in periodic structures have shown the existence of stop band and pass band regions in the frequency spectra [6-8]. Sound and vibration were forbidden in the stop bands of infinite periodic structures. This is of interest for applications such as frequency filters, noise absorbers, vibration absorbers, and high-precision mechanical systems [9-13]. Therefore, periodic structures can be applicable to noise and vibration control for their outstanding isolation effectiveness in the stop band regions. The stop band regions can be tailored to match the frequency bands that contained harmonics frequencies of vibration excitations, attenuating noise and vibration in these frequency bands [14]. To decrease power flow and power transmissibility of floating raft systems,

periodic structures were introduced to floating raft systems. A genetic algorithm (GA) was utilized to tailor the stop band regions of periodic structures in this study.

GAs are a kind of population-based search and optimization methods that mimic the process of natural evaluation. They have been successfully applied to various optimization problems which are difficult to be solved by conventional methods [15]. GAs have also been applied to a wide range of applications in noise and vibration control area, such as optimization of noise barriers [16], mufflers [17-19], supporting structures [20], and acoustical sandwich panels [21]. GAs have noticeable advantages of handling optimization problems which exist large numbers of parameters, multiple criteria, and parameters in discrete data series. Moreover, GAs are especially capable for optimization problems with many local optimal, which are unreliable for direct optimum methods (i. e. steepest ascent) [22]. The advantages of GAs are especially capable for solving the optimization problem in this study. Therefore, a GA was utilized in the design approach for periodic structures.

2. Theory

As shown in Fig. 1, a floating raft system consisted of five substructures: two identical machines (substructure 1), eight identical isolators (substructure 2), an intermediate raft (substructure 3), four identical periodic structures (substructure 4), and a simply supported flexible floor (structure 5) were considered in this study.

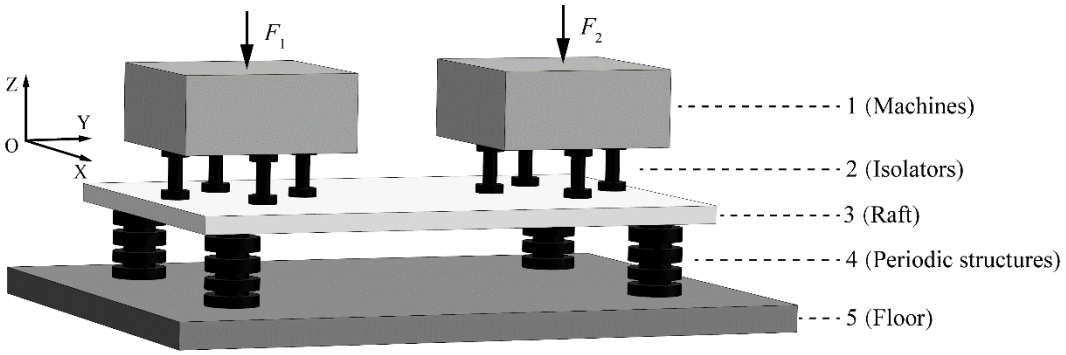

Fig. 1. A schematic diagram of the floating raft system.

2.1. Model of the periodic structures

It is assumed that each periodic structure in the floating raft consisted of $N1$ unit cells. Each unit cell consisted of $N2$ layers. The one-dimensional (1-D) model of a unit cell is shown in Fig. 2. The transfer matrix method was used to calculate the band gaps and wave transmission characteristics of 1-D periodic structure models because of its simplicity and convenience [23].

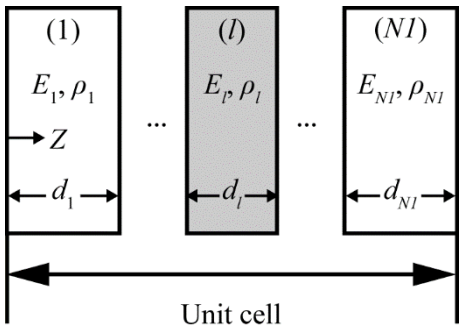

Fig. 2. A schematic diagram of a unit cell in a periodic structure.

The governing equation for the longitudinal wave propagated in the Z direction (as shown in Fig. 2) of the lth layer of a unit cell can be given as

$$\frac{\partial^2 u_l(z,t)}{\partial^2 t} = \frac{E_l}{\rho_l}\frac{\partial^2 u_l(z,t)}{\partial^2 z}, \tag{1}$$

where u_l denotes the displacement of the *l*th layer in a unit cell, ρ_l and E_l denote the density and Young's modulus of the material of the *l*th layer, respectively. The solution of Eq. 1 can be written as a superposition of forward and backward travelling waves with a harmonic time dependence

$$u(z,t) = \left[A_+^{(l)} e^{jk_p^{(l)} z} + A_-^{(l)} e^{-jk_p^{(l)} z} \right] \times e^{-jwt}, \tag{2}$$

where *j* denotes the imaginary unit; *w* denotes the angular frequency; $A_+^{(l)}$ and $A_+^{(l)}$ denote amplitudes of the forward and backward travelling waves, respectively; $k_p^{(l)} = \sqrt{w^2 \rho_l / E_l}$ denotes the wave number of the longitudinal wave in the *l*th layer of a unit cell.

The stress can be given as

$$\sigma(z,t) = E_l \frac{\partial u(z,t)}{\partial z}. \tag{3}$$

The transfer mobility model of the *l*th layer of a unit cell can be given as

$$\begin{bmatrix} u_{l+1} \\ \sigma_{l+1} \end{bmatrix} = \mathbf{TM}_{layer(l)} \begin{bmatrix} u_l \\ \sigma_l \end{bmatrix}, \tag{4}$$

$$\mathbf{TM}_{layer(l)} = \begin{bmatrix} \cos(k_p^{(l)} l_l) & -\dfrac{\sin(k_p^{(l)} l_l)}{E_l A_l k_p^{(l)}} \\ E_l A_l k_p^{(l)} \sin(k_l l_l) & \cos(k_p^{(l)} l_l) \end{bmatrix}, \tag{5}$$

where A_l and l_l denotes the cross-sectional area and the thickness of the *l*th layer.

The transfer mobility matrix between two connected unit cells can be given as

$$\begin{bmatrix} u_{p+1} \\ \sigma_{p+1} \end{bmatrix} = \mathbf{TM}_{cell} \begin{bmatrix} u_p \\ \sigma_p \end{bmatrix}, \tag{6}$$

$$\mathbf{TM}_{cell} = \prod_{l=1}^{N1} \mathbf{TM}_{layer(l)}. \tag{7}$$

The transfer matrix of the periodic structure can be given as

$$\mathbf{TM}_{ps} = (\mathbf{TM}_{cell})^{N2}. \tag{8}$$

The relationship between displacements and stress of two adjacent unit cells can be given as

$$\begin{bmatrix} u_{p+1} \\ \sigma_{p+1} \end{bmatrix} = \lambda \begin{bmatrix} u_p \\ \sigma_p \end{bmatrix}, \tag{9}$$

where $\lambda = e^{\mu} = e^{a+bj}$ denotes the propagation constant. Combining Eqs. (6) and (9), free wave propagated in the periodic structure can be described by the eigenvalue problem

$$\mathbf{TM}_{cell} \begin{bmatrix} u_p \\ \sigma_p \end{bmatrix} = \lambda \begin{bmatrix} u_p \\ \sigma_p \end{bmatrix}, \tag{10}$$

where $\lambda_1 = e^{\mu_1} = e^{a_1+b_1 j}$ and $\lambda_2 = e^{\mu_2} = e^{a_2+b_2 j}$ are eigenvalues of the transfer mobility matrix of a unit cell in the periodic structure. The real parts a_1 and a_2 describe the exponential decay rate of the longitudinal waves, whereas the imaginary parts b_1 and b_2 describe the phase transfer of the longitudinal waves through each unit cell [6]. If $a = 0$, the free waves propagate without attenuation, and the corresponding frequency bands are pass bands. If $a \neq 0$, the free waves propagate with attenuation, and the corresponding frequency bands are stop bands.

2.2. Model of the floating raft system

The transfer matrix models of the five substructures can be given as

$$\begin{Bmatrix} \mathbf{V}_i^t \\ \mathbf{V}_i^b \end{Bmatrix} = \mathbf{M}_i \begin{Bmatrix} \mathbf{F}_i^t \\ \mathbf{F}_i^b \end{Bmatrix} = \begin{bmatrix} \mathbf{m}_{11}^{(i)} & \mathbf{m}_{12}^{(i)} \\ \mathbf{m}_{21}^{(i)} & \mathbf{m}_{22}^{(i)} \end{bmatrix} \begin{Bmatrix} \mathbf{F}_i^t \\ \mathbf{F}_i^b \end{Bmatrix}, \ i=1\sim5, \tag{11}$$

where $\mathbf{V}_i^t$ and $\mathbf{F}_i^t$ denote the velocity and force vectors at connection points on the top interface of the *i*th substructure, respectively; $\mathbf{V}_i^b$ and $\mathbf{F}_i^b$ denote the velocity and

force vectors at connection points on the bottom interface of the *i*th substructure, respectively; $\mathbf{M}_i$ denotes the transfer mobility matrix between the velocity and force vectors of the *i*th substructure. It is assumed in this paper that the connections between different substructures were point connections.

The two identical machines were idealized by a rigid body model of uniform mass distribution. The mobility matrix of the machines can be given as [24]

$$\mathbf{m}_{11}^{(1)} = \left(1/\ jwm_1\right)\mathbf{I}_2, \quad \mathbf{m}_{12}^{(1)} = \frac{1}{jwm_1}\begin{bmatrix} 1_{1\times4} & 0_{1\times4} \\ 0_{1\times4} & 1_{1\times4} \end{bmatrix} \tag{12a, b}$$

$$\mathbf{m}_{21}^{(1)} = \left[\mathbf{m}_{12}^{(1)}\right]^{\mathrm{T}}, \quad \mathbf{m}_{22}^{(1)} = \frac{1}{jwm_1}\begin{bmatrix} \mathbf{s} & 0_{4\times4} \\ 0_{4\times4} & \mathbf{s} \end{bmatrix} \tag{12c, d}$$

$$\mathbf{s} = \begin{bmatrix} 1+\frac{m_1 d_1^2}{4J_1} & 1-\frac{m_1 d_1^2}{4J_1} & 1 & 1 \\ 1-\frac{m_1 d_1^2}{4J_1} & 1+\frac{m_1 d_1^2}{4J_1} & 1 & 1 \\ 1 & 1 & 1+\frac{m_1 d_1^2}{4J_1} & 1-\frac{m_1 d_1^2}{4J_1} \\ 1 & 1 & 1-\frac{m_1 d_1^2}{4J_1} & 1+\frac{m_1 d_1^2}{4J_1} \end{bmatrix}, \tag{12e}$$

where m_1 denotes the mass of a machine; $\mathbf{I}_2$ denotes a 2×2 identical matrix; the subscript T denotes the transpose of a matrix; d_1 denotes the distance between two opposite mounting points on the bottom interface of a machine; J_1 denotes the moment of inertial of a machine about its center of gravity.

The mobility matrix of the isolators can be given as

$$\mathbf{m}_{11}^{(2)} = \mathbf{m}_{22}^{(2)} = \left(\ jw/K_2 + 1/\ jwm_2\right)\mathbf{I}_8, \tag{13a}$$

$$\mathbf{m}_{12}^{(2)} = \mathbf{m}_{21}^{(2)} = \left(1/\ jwm_2\right)\mathbf{I}_8, \tag{13b}$$

where K_2 and m_2 denote the stiffness and mass of an isolator; $\mathbf{I}_8$ denotes a 8×8 identical matrix.

The mobility of mounting points on the intermediate raft can be solved by the modal summation method. The mobility matrix of the intermediate raft can be given as

$$\mathbf{m}_{11}^{(3)} = \left[\chi_{pq}(x_p^t, y_p^t \mid x_q^t, y_q^t) \right]_{8\times 8}, \tag{14a}$$

$$\mathbf{m}_{12}^{(3)} = \left[\chi_{pq}(x_p^t, y_p^t \mid x_q^b, y_q^b) \right]_{8\times 4}, \quad \mathbf{m}_{21}^{(3)} = \left[\mathbf{m}_{12}^{(3)} \right]^{\mathrm{T}} \tag{14b, c}$$

$$\mathbf{m}_{22}^{(3)} = \left[\chi_{pq}(x_p^b, y_p^b \mid x_q^b, y_q^b) \right]_{4\times 4}, \tag{14d}$$

$$\chi_{pq}(x_p, y_p | x_q, y_q) = jw \sum_{r=1}^{\infty} \frac{\phi_r(x_p, y_p)\phi_r(x_q, y_q)}{m_3 \left[w_r^2(1 + j\eta_3) - w^2 \right]}, \tag{14e}$$

where (x^t, y^t) and (x^b, y^b) denote coordinates of mounting points of an isolator and a periodic structure, respectively; m_3 and η_3 denote the mass and the loss factor of the intermediate raft, respectively; w_r denotes the *r*th order natural frequency of the intermediate raft; $\phi_r(x_p, y_p)$ and $\phi_r(x_q, y_q)$ denote the *r*th order natural modes of the intermediate raft at points (x_p, y_p) and (x_q, y_q), respectively.

The mobility matrix of the periodic structures can be given as

$$\mathbf{m}_{11}^{(4)} = -jwd / c \times \mathbf{I}_4, \tag{15a}$$

$$\mathbf{m}_{12}^{(4)} = jw / c \times \mathbf{I}_4, \tag{15b}$$

$$\mathbf{m}_{21}^{(4)} = jw(bc - ad) / c \times \mathbf{I}_4, \tag{15c}$$

$$\mathbf{m}_{22}^{(4)} = jwa / c \times \mathbf{I}_4, \tag{15d}$$

where a=$\mathbf{TM}_{ps}(1,1)$, b=$\mathbf{TM}_{ps}(1,2)$, c=$\mathbf{TM}_{ps}(2,1)$, d=$\mathbf{TM}_{ps}(2,2)$, and $\mathbf{I}_4$ denotes a 4×4 identical matrix.

The mobility matrix of the flexible floor can be given as

$$\mathbf{M}_5 = [\chi_{pq}(x_p, y_p | x_q, y_q)]_{4\times 4}, \tag{16a}$$

$$\chi_{pq}(x_p, y_p | x_q, y_q) = jw \sum_{n=1}^{\infty} \frac{\phi_n(x_p, y_p)\phi_n(x_q, y_q)}{m_5\left[w_n^2(1+j\eta_5) - w^2\right]}, \tag{16b}$$

where (x_p, y_p) and (x_q, y_q) denote coordinates of mounting points of the periodic structures on the flexible floor; m_5 and η_5 denote the mass and loss factor of the floor, respectively; w_n denotes the *n*th order natural frequency of the floor; $\phi_n(x_p, y_p)$ and $\phi_n(x_q, y_q)$ denote the *n*th order natural modes of the floor at points (x_p, y_p) and (x_q, y_q), respectively.

2.3. Analysis of power flow

The relationships between the transmitted forces and the corresponding velocities on the interfaces of the five substructures can be given as

$$\mathbf{F}_i^b = -\mathbf{F}_{i+1}^t, \ \mathbf{V}_i^b = \mathbf{V}_{i+1}^t, \ i = 1 \sim 4. \tag{17, 18}$$

By combining Eqs. (11) to (18), the force vector and the velocity vector of mounting points on the top interface of the flexible floor can be given as

$$\mathbf{F}_5^t = \mathbf{T}_4\mathbf{T}_3\mathbf{T}_2\mathbf{T}_1\mathbf{F}_1^t, \ \ \mathbf{V}_5^t = \mathbf{M}_5\mathbf{F}_5^t, \tag{19, 20}$$

where

$$\mathbf{T}_4 = -(\mathbf{M}_5 + \mathbf{m}_{22}^{(4)})^{-1}\mathbf{m}_{21}^{(4)}, \tag{21}$$

$$\mathbf{T}_i = -(\mathbf{m}_{11}^{(i+1)} + \mathbf{m}_{12}^{(i+1)}\mathbf{T}_{i+1} + \mathbf{m}_{22}^{(i)})^{-1}\mathbf{m}_{21}^{(i)}, \ i=1\sim 3. \tag{22}$$

The power flow through the periodic structures to the flexible floor can be given as [25]

$$P_f = \frac{1}{2}\mathrm{Re}((\mathbf{F}_5^t)^*\mathbf{V}_5^t). \tag{23}$$

The integral of power flow through the periodic structures to the flexible floor calculated over a given frequency band ($f_{\min}$, $f_{\max}$) can be given as

$$\overline{P}_f = \int_{f_{\min}}^{f_{\max}} \mathrm{Re}((\mathbf{F}_5^t(w))^* \mathbf{V}_5^t(w))dw . \tag{24}$$

The power transmissibility of the floating raft system can be expressed as [26]

$$\gamma = \frac{P_f}{P_m} = \frac{\mathrm{Re}((\mathbf{F}_5^t)^* \mathbf{V}_5^t)}{\mathrm{Re}((\mathbf{F}_1^t)^* \mathbf{V}_1^t)} . \tag{25}$$

3. The genetic algorithm optimization process

The aim of this paper was to minimize the integral of power flow through the periodic structures to the flexible floor calculated over a given frequency band. Two sets of geometrical parameters including the thicknesses and cross-sectional areas of layers in a unit cell that defined the dimensions of the periodic structures were considered in the optimization process. The thicknesses and sectional areas of layers in a unit cell can be expressed in the form of vectors, i. e. $\mathbf{d}$ = (d_1, d_2, …, d_l) and $\mathbf{A}$ = (A_1, A_2, …, A_l). Therefore, the integral of power flow through the periodic structures to the flexible floor calculated over a given frequency band was taken as the fitness function in this study, which can be given as

$$\text{Minimize } f = \overline{P}_f(\mathbf{d}, \mathbf{A}) . \tag{26}$$

In practice, there are always some limitations should be considered (i. e. the total thickness and the total mass of a design). In this study, the limitations of total thickness and mass were considered, which can be given as

$$N2 \times \sum_{l=1}^{N1} d_l \le d_{\max} , \tag{27}$$

$$N2 \times \sum_{l=1}^{N1} A_l \times \rho_l \times d_l \le M_{\max}, \tag{28}$$

where $d_{\max}$ and $M_{\max}$ were the maximum thickness and mass of a periodic structure.

A package of code for a genetic algorithm (GA) was utilized in the optimization process of this study for the noticeable advantages and suitability of GAs. The block diagram of the GA code utilized in this study is shown in Fig. 3.

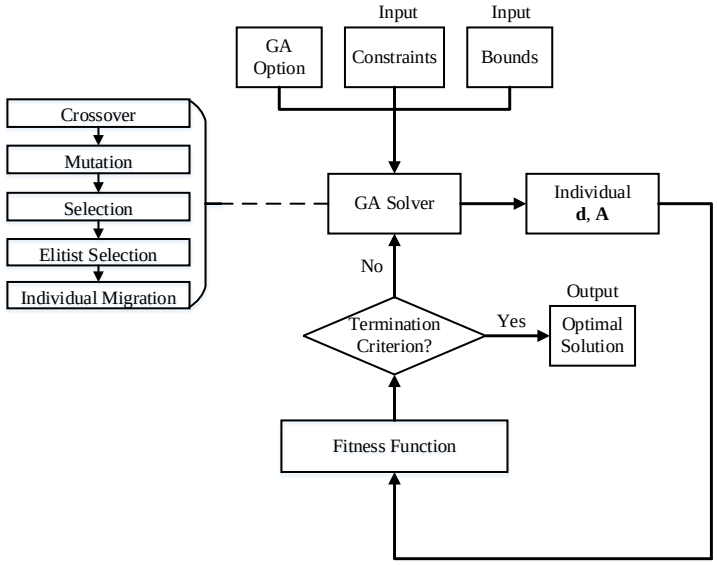

Fig. 3. A block diagram of the GA optimization algorithm.

As shown in Fig. 3, five bio-inspired operators: crossover, mutation, selection, elitist selection, and individual migration are included. Crossover and mutation are operations that changed binary data and gene values of chromosomes from individuals in one generation to individuals in another generation, respectively. Selection is the operation that chose excellent individuals for breeding the next generation individuals. Elitist selection is the operation that chose the best individuals to be passed to the next generation. Individual migration is the operation of re-grouping individuals from diverse populations.

4. Analysis

It has been shown that in practices if enough number of cells are available (usually three to four at least), structures consisted of periodic materials can exhibit similar wave attenuation characteristics to those of the periodic materials [10, 27-30]. A periodic structure with four unit cells were considered in this study. Each unit cell was consisted of two layers made of epoxy and steel.

The physical and geometrical parameters of the machines were m_1 = 30 kg, J_1 = 0.26 kg m^2, and d_1 = 0.2 m. The physical parameters of the isolators were m_2 = 0.25 kg, K_2 = 6.66×10^4 N/m. The physical parameters of the intermediate raft were m_3 = 75.6 kg, ρ_3 = 2.8×10^3 kg/m^3, E_3 = 2.1×10^{10} N/m^2, and η_3 = 0.02. The physical parameters of epoxy and steel used in the periodic structures (PS1) were ρ_{41} = 1.3×10^3 kg/m^3, E_{41} = 1.5×10^6 N/m^2, η_{41} = 0.08, ρ_{42} = 7.8×10^3 kg/m^3, E_{42} = 2.1×10^{11} N/m^2 and η_{42} = 0.04. The physical parameters of the flexible floor were m_5 = 567 kg, ρ_5 = 2.8×10^3 kg/m^3, E_5 = 2.1×10^{10} N/m^2, and η_5 = 0.02. The first order natural frequencies of the intermediate raft and the flexible floor were 82.5 Hz and 329 Hz, respectively.

Magnitude of the excitation force of a motor in the frequency band between 11 Hz and 500 Hz is shown in Fig. 4. The rotational speed of the motor is 3000 rotations per minute. It can be discerned that magnitude of the force contained peaks at 50 Hz (the rotational frequency of the motor) and harmonic frequencies of 50 Hz. It is assumed that magnitudes of the force at the top of the machines in the floating raft system were the same as the curve in Fig. 4.

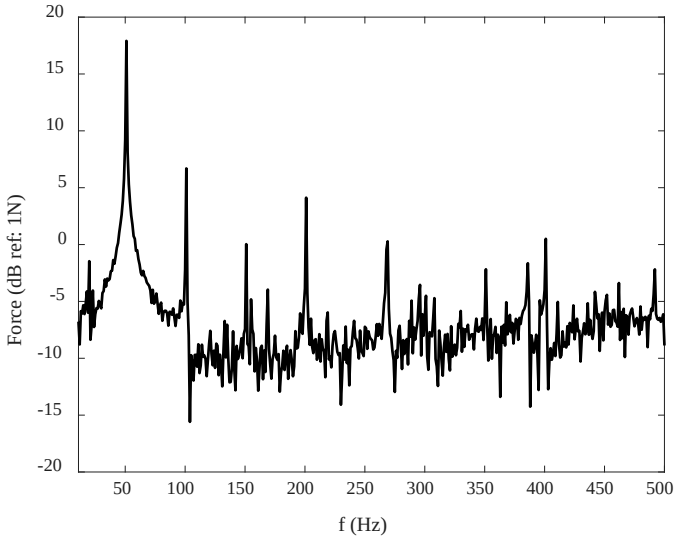

Fig. 4. Magnitude of the excitation force of a motor against frequency.

Identical periodic structures with geometrical parameters **d** = (0.07 m, 0.015 m) and **A** = (0.02 m^2, 0.04 m^2) were used in the floating raft system (FR1). The band structure of the periodic structure in the frequency range between 1 Hz and 500 Hz is shown in Fig. 5. The shaded areas, in the frequency ranges from 91 Hz to 242 Hz and from 276 Hz to 485 Hz of Fig. 5(b) stand for the stop band regions (phase of λ equals to 0 or π) of the periodic structures. The power transmissibility of the floating raft system is shown in Fig. 6. It shows obvious that, in the stop band regions, the power transmissibility reduced significantly.

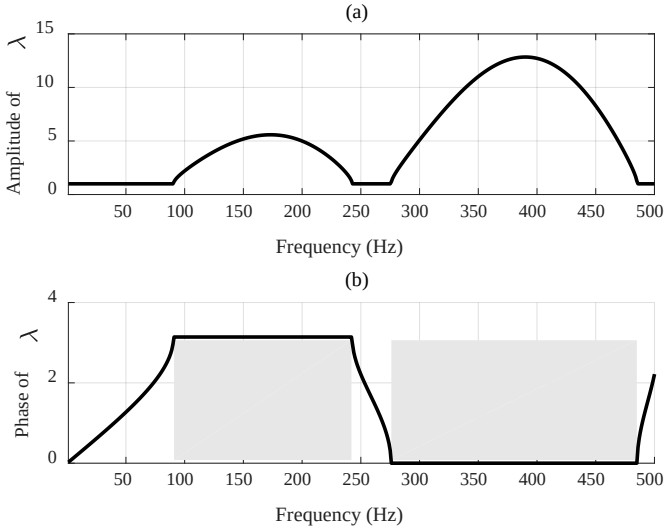

Fig. 5. Band structure of the periodic structures.

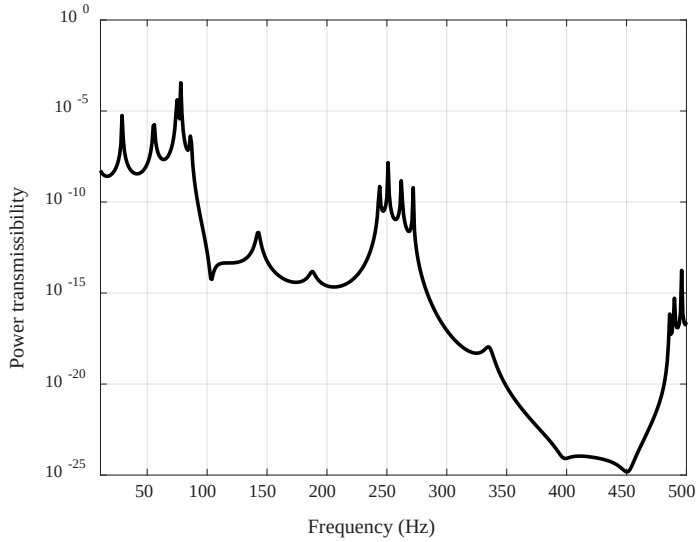

Fig. 6. Power transmissibility of the floating raft system FR1.

For a traditional floating raft system (FR2) with substructure 4 consisted of isolators but not periodic structures, the power flow and power transmissibility were also analyzed. The physical parameters of the isolators in substructure 4 of FR2 were m_4 = 0.4 kg, and K_4 = 3.01×10^5 N/m. The power flow of the flexible floors in the floating raft systems FR1 and FR2 are shown in Fig. 7. It can be found that the power

flow through the periodic structures to the flexible floor in FR1 were smaller than the power flow through the isolators to the flexible floor in FR2 in the stop band regions of the periodic structures (40 – 80 dB for most of the frequencies in the stop band regions of the periodic structures). In the pass band regions, the power flow through the periodic structures to the flexible floor in FR1 were larger than the power flow through the isolators to the flexible floor in FR2 (less than 10 dB for most of the frequencies in the pass band regions of the periodic structures). It can be concluded that if the stop band regions of periodic structures are tailored properly, the floating raft systems with periodic structures can be more effective than floating raft systems with isolators installed in substructure 4 in vibration control.

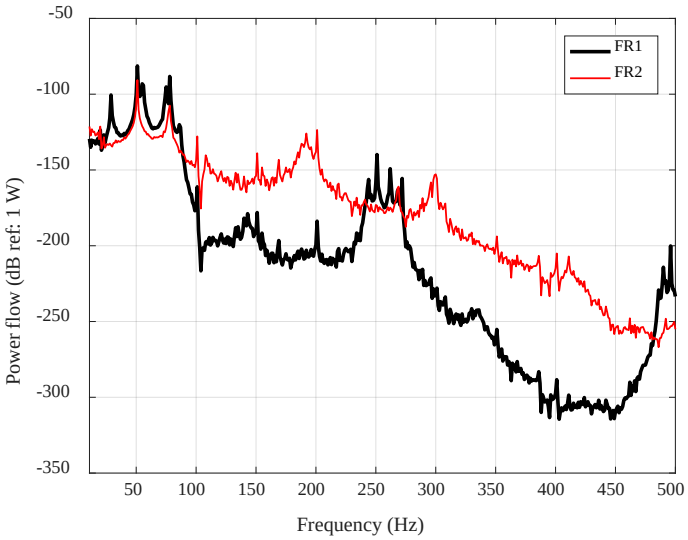

Fig. 7. Power flow through substructure 4 to the flexible floors in the floating raft systems FR1 and FR2.

4.1. The genetic algorithm options and the limitations

In this study, the values of the genetic algorithm (GA) options were: the population size *MP* = 10; the individual size *MI* = 40; the interval of migration *G* = 0.6; the rate of

crossover R_c = 0.75; the rate of mutation R_m = 0.01. The maximum number of generations M_g, the maximum number of generations of the GA executes without the optimization having reached convergence was 50.

In the optimization progress, the thicknesses of layers in a unit cell were in the range between 0.0025 m and 0.08 m with an increment of 0.0025 m. The cross-sectional areas of layers in a unit cell were in the range between 0.015 m^2 and 0.17 m^2 with an increment of 0.005 m^2. The integral of power flow through the periodic structures to the flexible floor calculated over the frequency band (11 Hz, 500 Hz) was taken as the fitness function in this optimization progress. Limitations of the periodic structures in this study were $d_{\max}$ = 0.5 m and $M_{\max}$ = 200 Kg.

4.2. Optimization of the periodic structures

In the GA optimization process, power flow through the periodic structures to the flexible floor in the frequency band between 11 Hz and 500 Hz were being focused on. During the GA optimization process, the values of the fitness function decreased rapidly and converged gradually after the first 20 generations. The first 50 generations of the convergence progress of the GA optimization is shown in Fig. 8. The geometric parameters for the optimum periodic structure (PS2) were **d** = (0.08 m, 0.045 m) and **A** = (0.015 m^2, 0.135 m^2). The band structure of the optimum periodic structure is shown in Fig. 9. The shaded areas of Fig. 8(b), in the frequency ranges from 25 Hz to 212 Hz, from 216 Hz to 424 Hz, and from 427 Hz to 500 Hz stand for the stop band regions. The rotational frequency (50 Hz) and all the harmonic frequencies of the machines were

in the stop band regions of the periodic structures. By comparing Fig. 5 with Fig. 9, it is obvious that the stop band regions were enlarged, especially for the first stop band region. The power transmissibility of the floating raft system (FR3) with the optimum periodic structures installed is shown in Fig. 10. It is obvious that power transmissibility of the floating raft with the optimum periodic structures installed was much smaller than power transmissibility in Fig. 6.

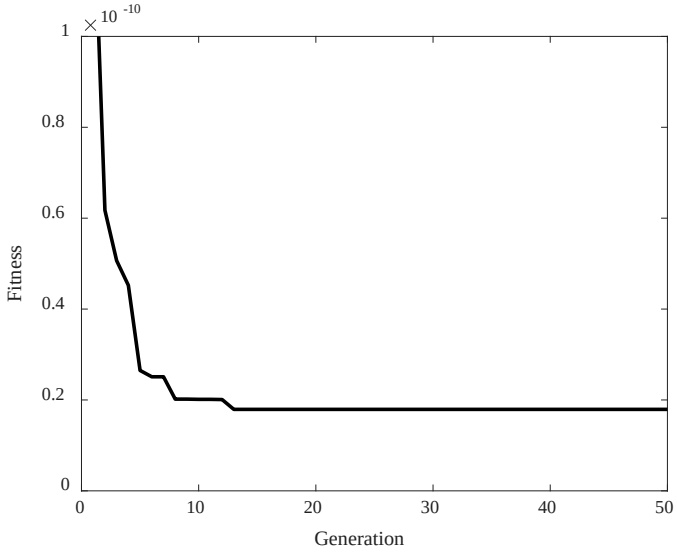

Fig. 8. The convergence progress of the GA optimization process.

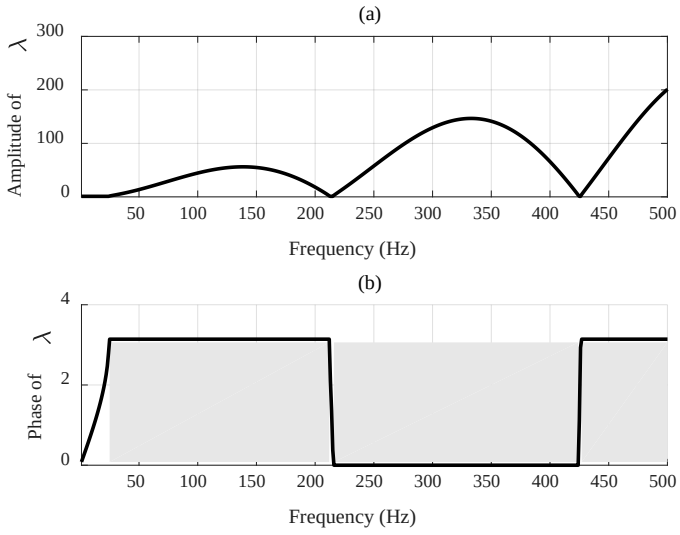

Fig. 9. Band structure of the optimum periodic structure.

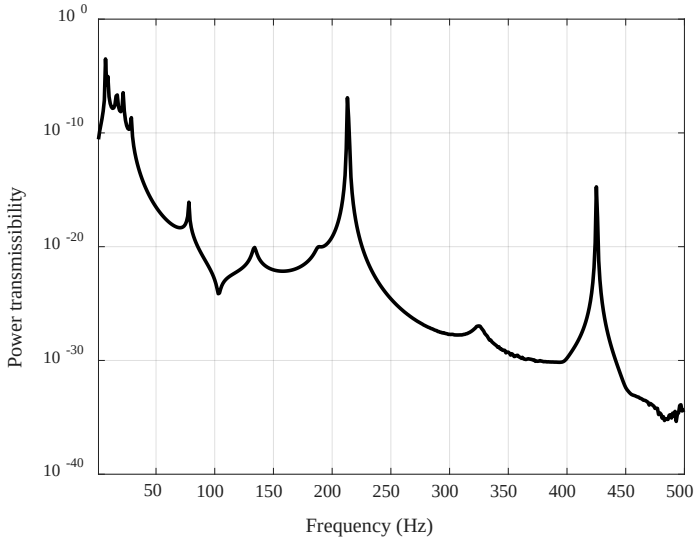

Fig. 10. Power transmissibility of the floating raft system with the optimum periodic structures installed.

The power flow through the periodic structures to the flexible floors in the floating raft systems FR1 and FR3 are shown in Fig. 11. The peak values of the power flow through the periodic structures to the flexible floors in FR1 and FR3 were -81.4 dB at 51 Hz and -112.1 dB at 17 Hz, respectively. In the stop band regions of the optimum periodic structure, the power flow through the optimum periodic structures to the flexible floor in FR3 were smaller than the power flow through the periodic structures to the flexible floor in FR1 (60 – 120 dB for most of the frequencies in the stop band regions of the optimum periodic structure). In the pass band regions of the optimum periodic structure, the power flow through the optimum periodic structures to the flexible floor in FR3 were larger than the power flow through the periodic structures to the flexible floor in FR1 (less than 20 dB for most of the frequencies in the pass band regions of the optimum periodic structure). It is obvious that the floating raft system FR3 have better isolation effectiveness than the floating raft system FR1. By comparing

Fig. 7 with Fig. 11, it is obvious that the floating raft system FR3 have better isolation effectiveness than the floating raft system FR2.

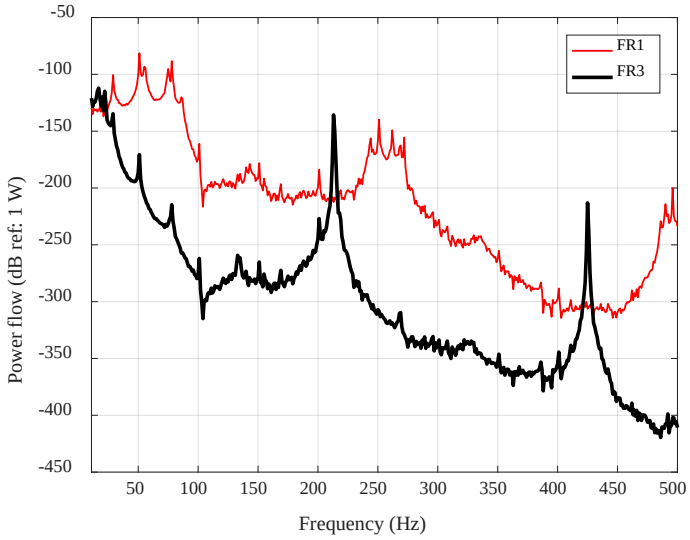

Fig. 11. Power flow through the periodic structures to the flexible floors in the floating raft systems FR1 and FR3.

5. Conclusions

In this paper, the application of periodic structures was presented to decrease the power transmissibility of a floating raft system. The band gap properties of the periodic structures and the power transmissibility of the floating raft system were investigated by using the transfer matrix method. The simulation results showed that the power transmissibility of the floating raft system decreased rapidly in the stop band regions of the periodic structures. It was validated that periodic structures can be an effective part of floating raft systems to decrease the power transmissibility of floating raft systems.

To minimize the integral of power flow through the periodic structures to a floating raft system calculated over a given frequency band, a design approach for optimizing

the geometrical parameters of the periodic structures was proposed. The geometrical parameters: thicknesses and cross-sectional areas of layers in periodical structures were optimized by using the genetic algorithm (GA). The fitness function utilized in the GA was the integral of power flow through the periodic structures to the flexible floor in the floating raft system calculated over a given frequency band.

A case study has shown that the GA optimization progress converged in a few generations. The numerical results demonstrated that the stop band regions of the periodic structure were enlarged and the power flow through the periodic structures to the flexible floor in the floating raft system was decreased after optimization. Moreover, for the given excitation force with multiple harmonic frequency components, the stop band regions of the optimized periodic structure contained all the harmonic frequency components of the excitation force. The proposed optimization approach was suitable for the design of periodic structures and vibration isolation systems such as floating raft systems.

Acknowledgements

The authors would like to thank the financial support of the Hong Kong Polytechnic University.

References

[1] Niu JC, Song KJ, Lim CW. On active vibration isolation of floating raft system. J Sound Vib 2005;285(1–2):391-406.

[2] Sun HL, Zhang K, et al. Application of dynamic vibration absorbers in floating raft system. Appl Acoust 2010;71(3):250-7.

[3] Elachi C. Waves in active and passive periodic structures: A review. Proceedings of the IEEE 1976;64(12): 1666-98.

[4] Mead DJ, Wave propagation in continuous periodic structures: research contributions from Southampton, 1964–1995. J Sound Vib 1996;190(3):495-524.

[5] Cremer L, Heckl M, Petersson, BAT. Structure-borne sound: structural vibrations and sound radiation at audio frequencies. Berlin: Springer Science & Business Media; 2005.

[6] Yun Y, Mak CM. A study of coupled flexural-longitudinal wave motion in a periodic dual-beam structure with transverse connection. J Acoust Soc Am 2009;126(1):114-21.

[7] Mak CM, Wang Z. Recent advances in building acoustics: An overview of prediction methods and their applications. Build Environ 2015;91:118-26.

[8] Jiang GS, Liu YC, et al. Transmission and radiation of acoustic oblique incident through tube arrays based on phononic crystals theory. Appl Acoust 2017;116:117-26.

[9] Xiao Y, Wen JH, et al. Flexural wave propagation in beams with periodically attached vibration absorbers: Band-gap behavior and band formation mechanisms. J Sound Vib 2013;332(4):867-93.

[10] Hussein MI, Hamza K, et al. Multiobjective evolutionary optimization of periodic layered materials for desired wave dispersion characteristics. Struct Multidiscip Optim 2006;31(1):60-75.

[11] Yu DL, Wen JH, et al. Vibration reduction by using the idea of phononic crystals in a pipe-conveying fluid. J Sound Vib 2008;318(1–2):193-205.

[12] Jin GY, Zhang CY, Ye TG, Zhou JL. Band gap property analysis of periodic plate structures under general boundary conditions using spectral-dynamic stiffness method. Appl Acoust 2017;121:1-13.

[13] Yu DL, Liu YZ, Wang G, Zhao HG, Qiu J. Flexural vibration band gaps in Timoshenko beams with locally resonant structures. J Appl Phys 2006;100(12):124901.

[14] Richards D, Pines DJ. Passive reduction of gear mesh vibration using a periodic drive shaft. J Sound Vib 2003;264(2):317-42.

[15] Tamaki H, Kita H, Kobayashi S. Multi-objective optimization by genetic algorithms: a review. Proceedings of IEEE International Conference on Evolutionary Computation, Nagoya: IEEE 1996:517-22.

[16] Baulac M, Defrance J, Jean P. Optimisation with genetic algorithm of the acoustic performance of T-shaped noise barriers with a reactive top surface. Appl Acoust 2008;69(4):332-42.

[17] Barbieri R, Barbieri N. Finite element acoustic simulation based shape optimization of a muffler. Appl Acoust 2006;67(4):346-57.

[18] Chiu MC, Shape optimization of multi-chamber mufflers with plug-inlet tube on a venting process by genetic algorithms. Appl Acoust 2010;71(6):495-505.

[19] Guo R, Wang LT, Tang WB, Han S. A two-dimensional approach for sound attenuation of multi-chamber perforated resonator and its optimal design. Appl Acoust 2017;127:105-17.

[20] Wang Z, Mak CM, Ou DY. Optimization of geometrical parameters for a supporting structure with two installed coherent machines. Appl Acoust 2017;127:15-23.

[21] Wang TG, Li S, Nutt SR. Optimal design of acoustical sandwich panels with a genetic algorithm. Appl Acoust 2009;70(3):416-25.

[22] Leardi R. Genetic algorithms in chemometrics and chemistry: a review. J Chemometr 2001;15(7):559-69.

[23] Guo Z, Sheng MP, Pan J. Effect of boundary conditions on the band-gap properties of flexural waves in a periodic compound plate. J Sound Vib 2017;395:102-26.

[24] Mak CM, Su JX. A study of the effect of floor mobility on structure-borne sound power transmission. Build Environ 2003;38(3):443-55.

[25] Fahy FJ, Gardonio P. Sound and structural vibration: radiation, transmission and response. New York: Academic; 2007.

[26] Yun Y, Mak CM. Power Transmission from two coherent machines to a dual-layer coupling floor structure. J Vib Control 2011;17(5):711-20.

[27] Cao WW, Qi WK. Plane wave propagation in finite 2-2 composites. J Appl Phys 1995;78(7):4627-32.

[28] Hussein MI, Hulbert GM, Scott RA. Band-Gap Engineering of Elastic Waveguides Using Periodic Materials. Proceedings of the 2003 ASME International Mechanic Engineering Congress and R&D Expo, Washington, DC: ASME 2003:799-807.

[29] Hussein MI, Hulbert GM, Scott RA. Effects of “Finiteness” on Wave Propagation and Vibration in Elastic Periodic Structures. Proceedings of the 2003 ASME

International Mechanic Engineering Congress and R&D Expo, Washington, DC: ASME 2004:437-47.

[30] Hussein MI, Hulbert GM, Scott RA. Dispersive elastodynamics of 1D banded materials and structures: analysis. J Sound Vib 2006;289(4):779-806.